Microwave-enhanced H_2O_2-based process for treating aqueous malachite green solutions: Intermediates and degradation mechanism

YongMing Ju [a], ShaoGui Yang [a,*], YouChao Ding [a,b], Cheng Sun [a,*], ChengGang Gu [a], Zhong He [a], Chao Qin [a], Huan He [a], Bin Xu [c]

[a] State Key Laboratory of Pollution Control and Resource Reuse, School of the Environment, Nanjing University, Nanjing 210093, PR China
[b] JiangSu Entry-Exit Inspection and Quarantine Bureau, Nanjing 210093, PR China
[c] College of Environmental Science and Engineering, Tongji University, Shanghai 200092, PR China

ABSTRACT

This work was originally performed to compare H_2O_2-based degradation of aqueous malachite green (MG) under microwave (MW)-enhanced and conventional heating (CH)-enhanced conditions, with the whole reaction courses traced by UV–vis spectrophotometer. The results showed that the higher discoloration rates of MG were available during MW-enhanced process, implying that the special heating way of MW might be more benefit for the generation of hydroxyl radicals than that of CH. Furthermore, major intermediates were separated and identified by HPLC–ESI-MS and GC–MS techniques. On the basis of 53 intermediates, degradation mechanism was deduced as follows: firstly, *N*-de-methylation reactions. Secondly, adduction reactions. Thirdly, decomposition of conjugated structure reactions of MG. Fourthly, removal of benzene reactions. Finally, open-ring reactions. Additionally, results revealed that microwave-enhanced H_2O_2-based treatment had more advantages, such as higher degradation efficiency, and no removal of catalyst after treatment.

© 2009 Elsevier B.V. All rights reserved.

1. Introduction

As promising technologies for treating dye-contaminated waters, titanium dioxide and UV (TiO_2/UV) [1–3], hydrogen peroxide and UV (H_2O_2/UV) [4–6] and photo-Fenton reactions (H_2O_2/Fe^{3+}/UV) [7–9], are the most widely employed advanced oxidation processes (AOPs) techniques for the treatment of various types of industrial wastewaters [7,10–12]. Whereas, either separation of catalysts and metal ions after reactions or lower efficiencies of H_2O_2/UV with extra ultraviolet generators, etc., greatly cumbered its further utilities. Accordingly, with the attempt of solving part of above shortcomings, exploring new techniques would have far-reaching influences on both AOPs techniques and wastewater treatments.

Microwave technique has found its place in domestic, industrial and medical applications, such as polymerization and dehydration processes of organic synthesis, inorganic synthesis, analyses and extraction and food sterilization. Even since Florian and Knapp [13] proposed a novel procedure for the decomposition of interfering dissolved organic carbon and Satoshi [14] subsequently developed integrated microwave/UV–vis illumination technique, the utilities with the combination of microwave irradiation and other relevant hybrid techniques have been one of the preponderant hotspots in environmental remediation. For example, microwave-assisted photocatalytic and microwave-assisted catalytic wet air oxidation treatments have clearly demonstrated higher degradation efficiencies through treating pesticides [15,16], dyes [17,18], phenols [19–21] with catalysts and treating petroleum refinery wastewater [22], dyeing [23] and hazardous organic in wastewater [24]. However, obvious limitations include both manufacture of elecrodeless discharge lamps (EDLs) with specific emission spectral bands and separation of catalyst after degradation. However, MW-enhanced H_2O_2-based treatment could avoid or solve above-mentioned shortcomings with H_2O_2 as clean oxidants, whose high popularity and environmental acceptability has been greatly expanded to be performed under mild conditions in scope and scale. Nowadays, MW-enhanced H_2O_2-based treatment has been merely found on treatment of sludge [25–29]. Especially about treating mechanism or reaction routes discussion, only Cigdem et al. [29] once reported that elevated MW temperatures increased decomposition of H_2O_2 into hydroxyl radicals during synergetic pretreatment of sewage sludge with H_2O_2. To our best knowledge, the utility about MW-enhanced H_2O_2-based treatment without catalysts in wastewater treatment should be feasible. Therefore, we have chosen MW-enhanced H_2O_2-based treatment to tentatively discolorate malachite green (MG), an extensively used cationic triphenylmethane dye with genotoxic and carcinogenic properties [30,31]. The focus was concentrated on below aspects: (1)

Fig. 1. The whole apparatus used in MW (MW)-enhanced and CH-enhanced H_2O_2-based conditions.

Fig. 2. Variations of temperature within aqueous MG solution and pure water under MW irradiation condition.

exploring potential possibility about MW-enhanced H_2O_2-based treatment for wastewater through comparing MW-enhanced and CH-enhanced H_2O_2-based treatments to investigate the higher effectiveness of the former. (2) Identifying intermediates via GC–MS and LC–MS techniques and proposing MW-enhanced H_2O_2-based degradation mechanism.

2. Experimental

2.1. Reagents and materials

MG ($C_{23}H_{25}N_2Cl$) was purchased from Sigma Company. HPLC-grade ammonium acetate, acetate acid and acetonitrile were purchased from Tedian Company. H_2O_2 (30%, w/w) was purchased from Beijing Chemistry Co. De-ionized water was purified with a Milli-Q water ion-exchange system (Millipore Co.) to give a resistivity of $1.8 \times 10^7 \, \Omega$ cm.

2.2. Apparatus

All experiments were accomplished in a modified Midea MW oven (in Fig. 1) with initial concentration of MG as 100 mg/L and detail modifications were present as follows: drilled a hole in the upper oven wall and then attached an aluminum tube of the same diameter to the hole, through which a glass tube was attached connecting a water-cool condenser and a Pyrex vessel on its both sides. When the vessel was filled with 30 mL aqueous solution and connected to water-cooling condenser systems and MW power was adjusted to a maximal value (900 W, 2450 MHz) to guarantee continuous MW radiation, the reactor began to work and the solution for measurement could be obtained in time. Besides, a Pt-temperature transmitter was utilized to detect variation of solution temperature during degradation process and variations of microwave-irradiated solution temperature were displayed in Fig. 2, which could ensure that the final temperature of conventional heating way was properly and strictly controlled at 100 °C with 2% error. The leakage of MW oven is kept below 0.5 mW/cm² at 2450 MHz, which is measured at 20 cm distance from the aperture and is within the limit on the safe stray leakage of MW power density.
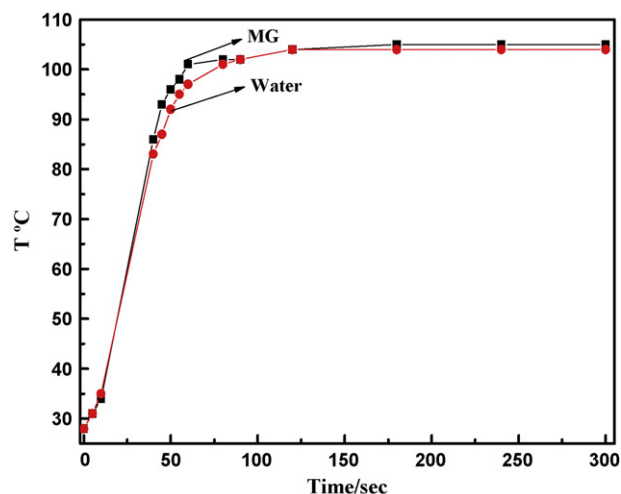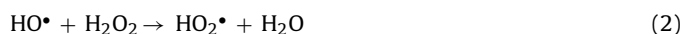
2.3. Experimental procedures and analysis methods

After setting interval time for degradation, samples were drawn for the analysis of UV–vis spectra, high performance liquid chromatography (HPLC), liquid chromatography electrospray ionization mass spectrometry (LC–ESI-MS). The detailed information about LC–ESI-MS and gas chromatography–mass spectrometry (GC–MS) referred to our previous study [32]. The measurement with modified HPLC method was performed with an acetonitrile/water = 50:50 (v/v) as mobile phase at a flow rate of 1 mL/min and detection wavelengths of 618 and 366 nm.

3. Results and discussions

3.1. Control experimental

The CH-enhanced H_2O_2-based reaction routes have been referred [33] and MW-enhanced H_2O_2-based reaction routes could be available in formal (1)–(3):

$$H_2O_2 \rightarrow 2HO^\bullet \tag{1}$$

$$HO^\bullet + H_2O_2 \rightarrow HO_2^\bullet + H_2O \tag{2}$$

$$2HO_2^\bullet \rightarrow H_2O_2 + O_2 \tag{3}$$

To demonstrate the roles of microwave irradiation and H_2O_2, and the relationship between MW-initiated and CH-initiated heating way, several sets of experiments were performed and corresponding results (in Fig. 3) are displayed below. Firstly, no decline of MG occurred with microwave irradiation alone, due to that the energy of microwave at frequency 2.45 GHz was not enough to destroy any bonds of MG. Secondly, the MW-enhanced degradation efficiency was higher than CH-enhanced degradation efficiency with the same input of H_2O_2, accompanying with a nonlinear effect between dosage of H_2O_2 and discoloration rates, although the discoloration rates increased with adding of the dosage of H_2O_2 under MW-enhanced and CH-enhanced process. Furthermore, the ratio about discoloration during MW-enhanced and CH-enhanced process was maximal with input about 30 mmol/L H_2O_2, implying that too much dosage of H_2O_2 might take negative effect on degradation of MG and the different heating way affected the generated concentration of hydroxyl radicals [29] for the discoloration of MG. For example, CH-based heat was transformed through heat transfer with more heat loss, which could generate thermal gradient. Meanwhile, MW-based heat could be carried out through the col-
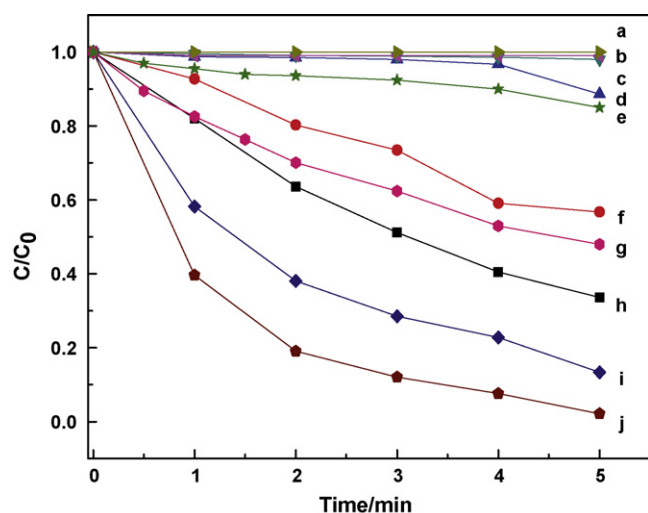
Fig. 3. Variations of MG were displayed under different conditions. (a) MW, (b) thermal, (c) CH/H_2O_2-3, (d) CH/H_2O_2-30, (e) MW/H_2O_2-3, (f) CH/H_2O_2-150, (g) MW/H_2O_2-30, (h) CH/H_2O_2-300, (i) MW/H_2O_2-150, (j) MW/H_2O_2-300.

lision of polar groups, which could accomplish bulk phase heating at the same time and affect polar molecular motion and attack of hydroxyl radicals. Additionally, the higher degradation efficiencies implied that MW-enhanced treatment could be utilized to treat industrial dye wastewater with advantages, such as no removal of catalyst.

3.2. UV–vis spectra

To trace the whole reaction routes, UV–vis spectrophotometer was utilized to acquire UV–vis spectra of solutions. Variations of MW-enhanced and CH-enhanced H_2O_2-based absorption spectra of MG with the same input amount of H_2O_2 were shown in Fig. 4 and absorption spectra partly enlarged (500–700 nm) was also illustrated in the inset of Fig. 4.

Great similarities with obvious newly produced absorbance at about 360 nm and no obvious blue-shift at about 618 nm disclosed the similar degradation courses. According to our previous research [32], attack on central carbon could generate DLBP as one of the main products with obvious absorbance at 360 nm and N-de-methylated reaction could generate blue-shift at about 618 nm. Thus, the results in Fig. 4 suggested that not N-de-methylated reaction but attack on central carbon at different reaction rates could be deduced as dominant reaction courses under both MW-

enhanced and CH-enhanced H_2O_2-based process, although the blue-shift numbers were identified as $\Delta\lambda = 2$ nm (618–616 nm) under CH-enhanced condition and $\Delta\lambda = 3$ nm (618–615 nm) under MW-enhanced condition, separately.

3.3. Chromatography of HPLC under MW-enhanced and CH-enhanced H_2O_2-based processes

All information about chromatography of HPLC has been depicted in Figs. 5 and 6, which could be utilized to quantify main products. The peak with $t_R = 4.829$ min was identified as MG (in Fig. 5) through comparing the retention time (t_R) and corresponding spectral analysis with that of standard substance. According to spectra analysis of corresponding peaks with $t_R = 3.537$, 3.936, 4.829, 6.449 and 6.862 min, these intermediates were identified as N-de-methylated products, implying that N-de-methylated reactions were presented within CH-enhanced condition. According to corresponding peaks with $t_R = 3.936$ and 4.829 min within MW-enhanced condition, similar phenomena were observed. The spectra of peak with $t_R = 1.653$ min differed from others (in Fig. 5), which might be carbinol base of malachite green to be identified further. The amounts of intermediates peaks detected at 618 nm in CH-enhanced courses (in Fig. 5), were more than those in MW-enhanced courses, which could be attribute to that N-de-methylated products could be quickly degraded by higher concentration of MW-based hydroxyl radicals [33].

Besides, another proceeding reaction route was the decomposition of central carbon reactions (in Fig. 6), accompanying with a new intermediate with max absorbance at about 360 nm. This intermediate was identified as 4-dimethylaminobenzophenone (DLBP) [34] with $t_R = 10.078$ min, which could be further degraded into a series of intermediates with $t_R = 2.986$, 3.278, 4.125, 4.608, 6.196 and 8.816 min in HPLC chromatography. Thus, obvious blue-shift phenomenon in corresponding UV–vis spectra (in Fig. 6A) were anatomizing with variations of UV-spectra in Fig. 4. Similar reaction courses were observed during CH-enhanced process (in Fig. 6B). The main products with $t_R = 6.198$ and 10.076 min could also be generated through above-mentioned routes, implying attack of hydroxyl radicals on central carbon with a series of intermediates to form corresponding blue-shift. Moreover, unknown product with $t_R = 2.130$ min was different from others. All corresponding information in Figs. 5 and 6 implied that attack on central carbon reactions were main reaction routes within both conditions.

Although N-de-methylation courses [35,36] were once believed as the main steps in photodegradation, relative peak area of main intermediates in HPLC has clearly demonstrated that decomposi-
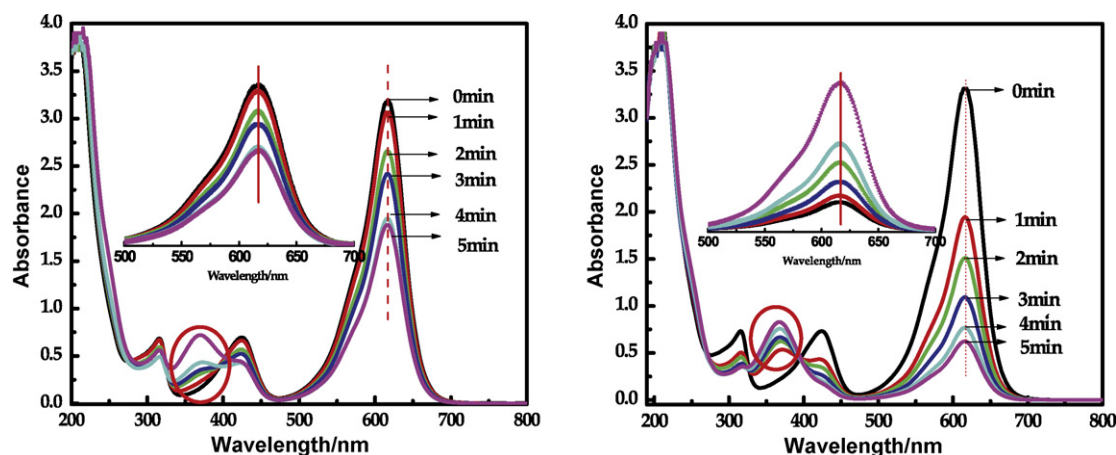

Fig. 4. UV–vis spectra of MG under different conditions: (A) CH/H_2O_2-150 and (B) MW/H_2O_2-150 (the insets were absorption spectra enlarged (500–700 nm)).
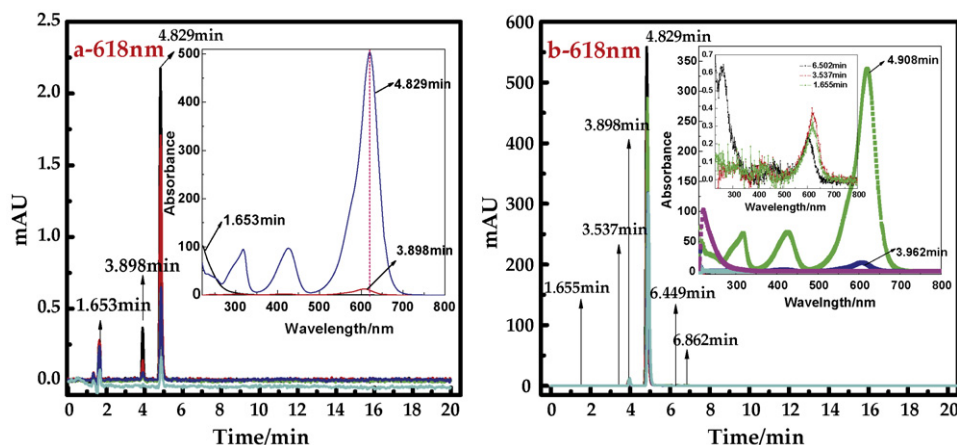
Fig. 5. Chromatography of HPLC with UV–vis spectra of corresponding peaks under (a) MW-enhanced and (b) CH-enhanced conditions, detected at 618 nm.

tion of conjugated structure of MG might be the main reaction routes during both H_2O_2-beased processes. Besides, according to comparison about UV–vis spectra in Figs. 5 and 6, the different concentration of generated hydroxyl radicals under both conditions resulted in differences of degradation courses, especially the reaction routes and intermediates.

4. Reaction mechanism under MW-enhanced condition

4.1. Identification of intermediates and some isomers

The total ion chromatogram (TIC) of LC–MS was displayed in Fig. 7. All intermediates detected by LC–MS and GC–MS (in Tables 1 and 2), could be divided into five families:

(1) The intermediates from B to F, were generated through N-de-methylation reactions. The results of mass spectral analysis confirmed that the component A, $m/z = 329.3$ is MG. The other components are B, $m/z = 315.3$ [32,34]; C, $m/z = 301.5$; D, $m/z = 287$; E, $m/z = 273$; F, $m/z = 258$; G, $m/z = 243$.

(2) The intermediates from a to f, were produced either through hydroxylated reaction of N-de-methylated products or through hydroxylated reactions of MG, following with N-de-methylated reactions. The results of mass spectral analysis confirmed that the component a, $m/z = 345$ [37]; b, $m/z = 331$; c, $m/z = 317$; firstly detected component d, $m/z = 303$; e, $m/z = 289$; f, $m/z = 274$; g, $m/z = 259$.

The intermediates from a_1 to f_1, were produced either through adduction reaction at a ratio of 2:1 between hydroxyl radicals and N-de-methylated products, or through adduction
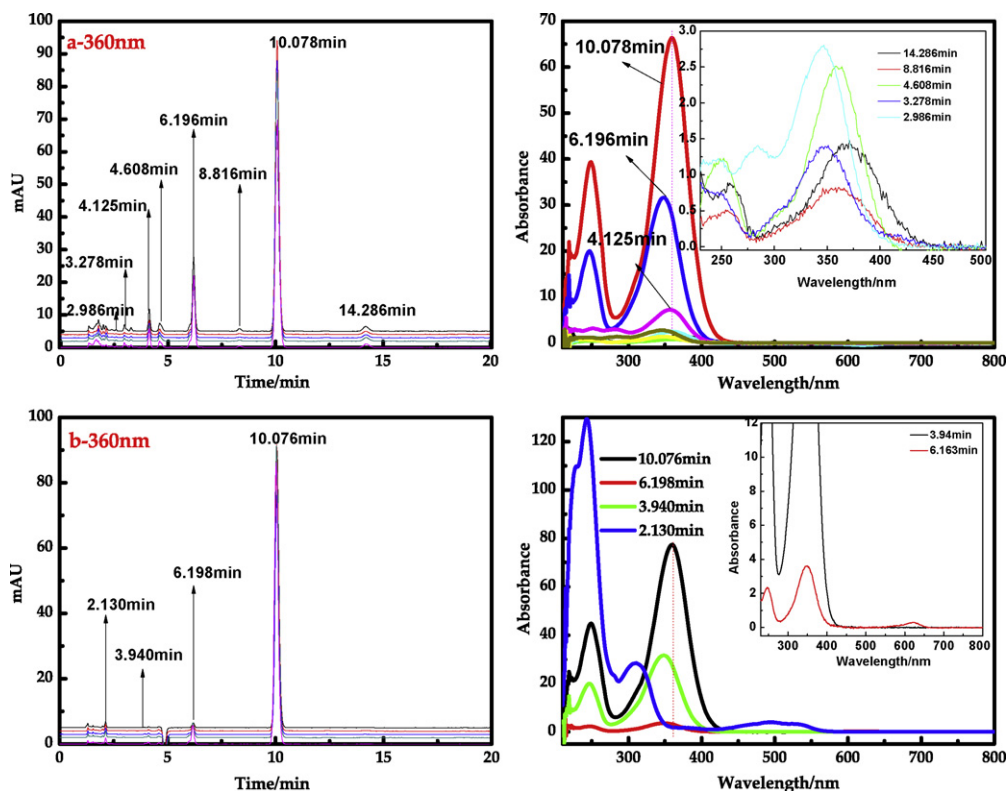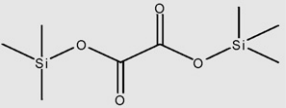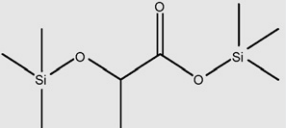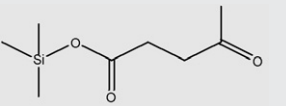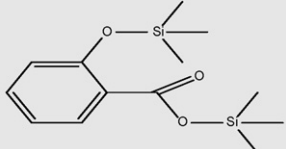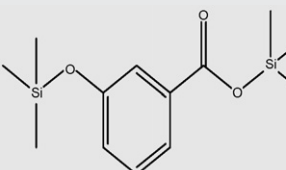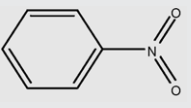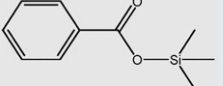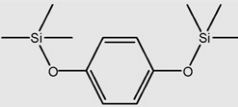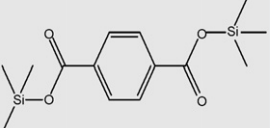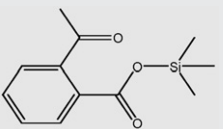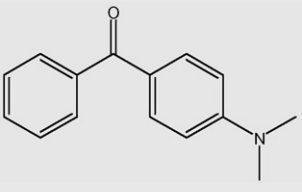

Fig. 6. Chromatography of HPLC with UV–vis spectra of corresponding peaks under (a) MW-enhanced and (b) CH-enhanced conditions, detected at 360 nm.

Table 1
Identified products and main fragments determined by GC–EI-MS.

Retention time(min)	Structure of derivatives	Derivatives' fragments (m/z, %)	Corresponding product
3.859		45 (40); 73 (100); 147 (95)	b_{11}
3.864		45 (40); 73 (100); 147 (95); 191 (20)	b_{12}
4.126		45 (40); 75 (100); 173 (40)	b_{13}
4.509		73 (100); 135 (15); 267 (90)	a_{13}
4.549		73 (20); 73 (60); 193 (50); 223 (40); 267 (100); 282 (40)	a_{14}
5.813		51 (60); 77 (80); 105 (100); 123 (40)	a_{15}
5.854		51 (50); 77 (70); 105 (100); 123 (30)	a_{12}
6.920		73 (60); 239 (100); 254 (75)	a_{17}
9.934		73 (20); 103 (20); 221 (25); 295 (100)	a_{16}
11.048		50 (20); 76 (30); 149 (100)	a_{11}
12.827		51 (20); 77 (40); 105 (20); 148 (100); 225 (60)	a_3

Fig. 7. TIC of LC/MS after 3 min degradation under MW-enhanced process. A–D represents DM-PM, DMPPM, MG, DLBP, separately.

Table 2
Products and main fragments determined by HPLC–ESI-MS.

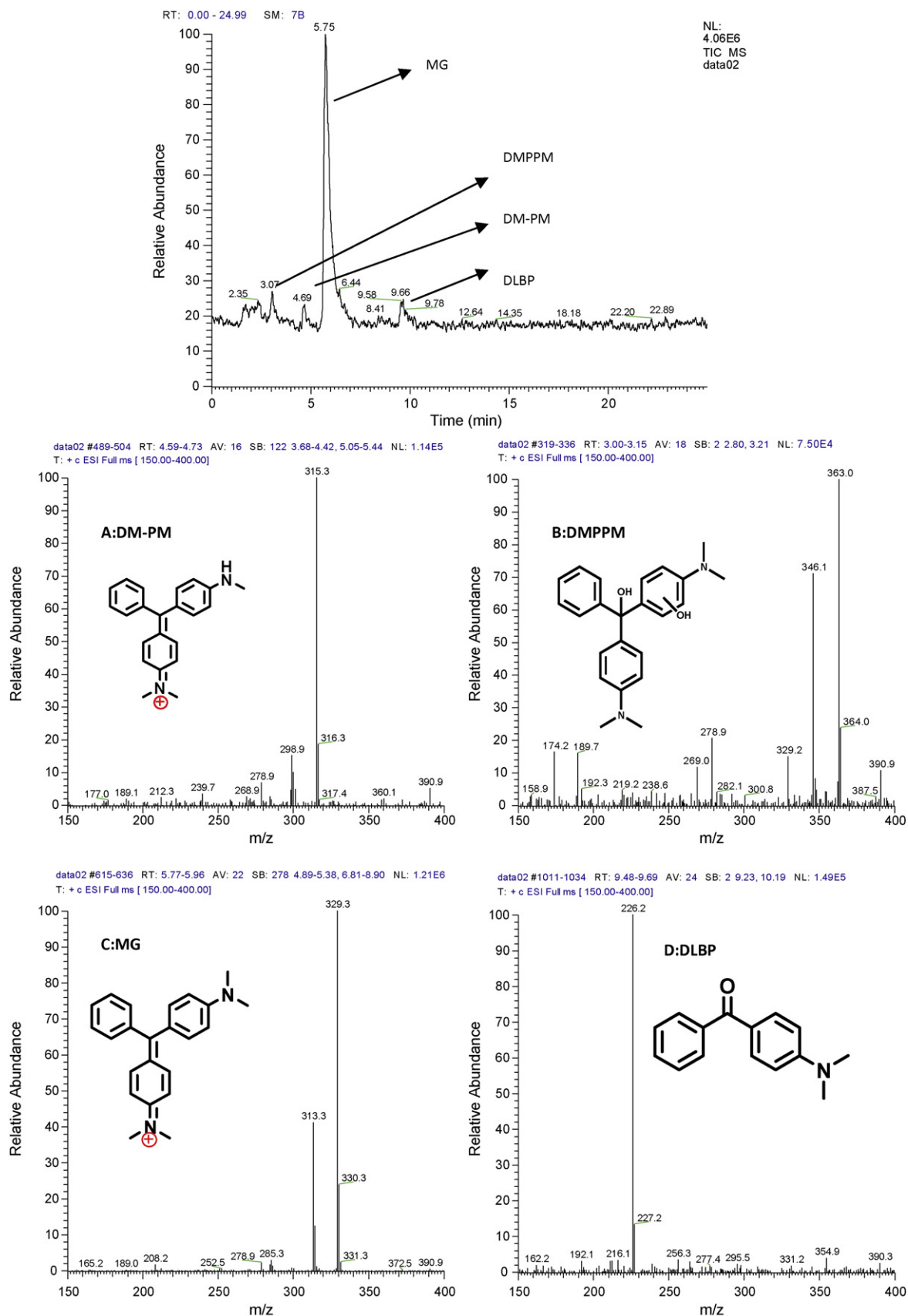| Peak	Compound	Retention time (min)	m/z	ESI/MS
A	M	3.09	329	329.3
B	M−CH$_2$	2.47	315	315.3
C	M−2CH$_2$	6.22	301	300.8
D	M−3CH$_2$	6.16	287	287.6
E	M−4CH$_2$	6.18	273	273.5
F	M−4CH$_2$−NH	6.41	258	258.3
a	M+OH	3.09	345	345.8
b	M+OH−CH$_2$	2.45; 3.10; 6.88	331	331.4
c	M+OH−2CH$_2$	2.48; 3.84; 6.26	317	317.2
d	M+OH−3CH$_2$	7.43	303	303.8
e	M+OH−4CH$_2$	6.47	289	289.4
f	M+OH−4CH$_2$−NH	6.31	274	274.2
a$_1$	M+2OH	2.69; 6.22	361	361.4
b$_1$	M+2OH−CH$_2$	3.10	347	347.6
c$_1$	M+2OH−2CH$_2$	2.48; 6.24	333	333.2
d$_1$	M+2OH−3CH$_2$	2.14; 4.04;	319	319.0; 319.9
e$_1$	M+2OH−4CH$_2$	6.33;	305	305.6
f$_1$	M+2OH−4CH$_2$−NH	4.75;	290	290.2
a$_2$	M+3OH	6.26	378	378.1
b$_2$	M+3OH−CH$_2$	3.09	364	362.9
c$_2$	M+3OH−2CH$_2$	5.28	350	348.9
d$_2$	M+3OH−3CH$_2$	6.28	336	334.2
e$_2$	M+3OH−4CH$_2$	6.32	322	320.9
a$_3$	D	9.86	225	225.8
b$_3$	D−CH$_2$	6.03	211	211.8
c$_3$	D−2CH$_2$	6.05	197	197.1
d$_3$	D−2CH$_2$−NH	1.72	182	181.9
a$_4$	D+OH	2.37	241	241.8
b$_4$	D+OH−CH$_2$	9.88	227	226.3
c$_4$	D+OH−2CH$_2$	6.03	213	212.2
d$_4$	D+OH−2CH$_2$−NH	6.05	198	198.1
a$_5$	D+2OH	3.92	257	257.1
b$_5$	D+2OH−CH$_2$	2.35	243	243.1
c$_5$	D+2OH−2CH$_2$	9.89	229	228.2
d$_5$	D+2OH−2CH$_2$−NH	6.15	214	214.2

reaction at a ratio of 2:1 between hydroxyl and MG, following with N-de-methylation reactions. The results of mass spectral analysis confirmed that the component a$_1$, m/z = 361 [36]; b$_1$, m/z = 347; and firstly detected c$_1$, m/z = 333; d$_1$, m/z = 319; e$_1$, m/z = 305; f$_1$, m/z = 290; g$_1$, m/z = 275.

The intermediates from a$_2$ to f$_2$, were produced either through adduction reaction at a ratio of 3:1 between hydroxyl radicals and N-de-methylated products, or through adduction reactions at a ratio of 3:1 between hydroxyl radicals and MG, following with N-de-methylation reactions. The results of mass spectral analysis confirmed that the component a$_2$, m/z = 378 [37]; b$_2$, m/z = 364 [37]; c$_2$, m/z = 350; d$_2$, m/z = 336; e$_2$, m/z = 322.

(3) The intermediate a$_3$ was produced through the decomposition of conjugated structure of MG, which could be further degraded through N-de-methylation reactions. The results of mass spectral analysis confirmed that the N-de-methylated component a$_3$, m/z = 225 [37]; b$_3$, m/z = 211 [37]; c$_3$, m/z = 197 [37]; d$_3$, m/z = 182 [37]. The intermediates from a$_4$ to d$_4$, were generated either through adduction reaction at a ratio of 1:1 between hydroxyl radicals and N-de-methylation products of a$_3$, or through adduction reaction at a ratio of 1:1 between hydroxyl radicals and a$_3$, following with N-de-methylation reactions. The results of mass spectral analysis confirmed that the component a$_4$, m/z = 241; b$_4$, m/z = 227; c$_4$, m/z = 213; d$_4$, m/z = 198. The intermediates from a$_5$ to d$_5$, were generated either through adduction reaction at a ratio of 2:1 between hydroxyl radicals and N-de-methylated products of a$_4$, or through adduction reaction at a ratio of 2:1 between hydroxyl radicals and a$_4$, following with N-de-methylation reactions. The results of mass spectral analysis confirmed that the component a$_5$, m/z = 257;

b$_5$, m/z = 243; c$_5$, m/z = 229; d$_5$, m/z = 214.

(4) The intermediates from a$_{11}$ to a$_{18}$, identified by GC–MS, were produced through the removal of benzene reactions. The results of mass spectral analysis confirmed the major ions of component a$_{12}$ with t_R = 5.854 min in the mass spectra, include (m/z, %): 51 (50; C$_4$H$_3^+$); 77 (70; C$_6$H$_5^+$); 105 (100; (M−OH)$^+$); 122 (30; M$^+$). The major ions of component a$_{14}$ with t_R = 4.549 min in the mass spectra, include (m/z, %): 73 (60; (CO$_2$HSi)$^+$); 193 (50; (M+H$^+$−6CH$_3$)$^+$); 223 (40; (M+H$^+$−4CH$_3$)$^+$); 267 (100; (M−CH$_3$)$^+$); 282 (40; M$^+$). The major ions of component a$_{13}$ with t_R = 4.509 min in the mass spectra, include (m/z, %): 73 (100; (CO$_2$HSi)$^+$); 267 (90; (M−H)$^+$). The major ions of component a$_{16}$ with t_R = 9.934 min in the mass spectra, include (m/z, %): 73 (20; (CO$_2$HSi)$^+$); 103 (20); 221 (25; (M−H−5CH$_3$)$^+$); 295 (100; (M−H)$^+$). The major ions of component a$_{17}$ with t_R = 6.920 min in the mass spectra, include (m/z, %):73 (60; (CO$_2$HSi)$^+$); 239 (100; (M−CH$_3$)$^+$); 254 (75; M$^+$). The major ions of component a$_{11}$ with t_R = 11.048 min in the mass spectra, include (m/z, %): 50 (20); 76 (30; C$_6$H$_4^+$); 149 (100; (M−H)$^+$). The major ions of component a$_{15}$ with t_R = 5.813 min in the mass spectra, include (m/z, %): 51 (60); 77 (80; C$_6$H$_5^+$); 105 (100; (M−OH)$^+$); 123 (40; M$^+$).

(5) The intermediates from b$_{11}$ to b$_{13}$, identified by GC–MS, were produced through open-ring reactions. The results of mass spectral analysis confirmed that the major ions of component b$_{11}$ with t_R = 3.859 min in the mass spectra, include (m/z, %): 45 (40); 73 (100; (CO$_2$HSi)$^+$); 147 (95; C$_2$O$_4$Si$_2$H$^+$). The major ions of component b$_{12}$ with t_R = 3.864 min in the mass spectra, include (m/z, %): 45 (40); 73 (100; (CO$_2$HSi)$^+$); 147 (95; (M−5CH$_3$−2H)$^+$); 191 (20; (M−2CH$_3$−H)$^+$). The major ions of component b$_{13}$ with t_R = 4.126 min in the mass spectra, include (m/z, %): 45 (40); 75 (100; (CO$_2$H$_3$Si)$^+$); 173 (40; (M−H)$^+$).

The isomers of b with t_R = 2.45, 3.10 and 6.88 min, were produced through adduction reaction at a ratio of 1:1 between hydroxyl radical and MG, following with one N-de-methylation reaction. The isomers of c with t_R = 2.48, 3.84 and 6.26 min, were produced through adduction reaction at a ratio of 1:1 between hydroxyl radical and MG, following with N-de-methylation reactions.

The isomers of c$_1$ might arise from the N-de-methylation reactions at different position with retention time at 2.48 and 6.24 min. The compounds of d$_1$ with t_R = 2.14 and 4.04 min were produced through adduction reaction at a ratio of 2:1 between hydroxyl radicals and a$_1$, following with N-de-methylation reactions at different positions.

4.2. Degradation mechanisms of MG

Previous research has provided some degradation mechanism. Chen [34] et al. thought photodegradation of MG is favorable to cleavage of whole conjugated chromophore structure under acidic conditions and N-de-methylated reactions are preferred under basic conditions. Zhao et al. [38] proposed that degradation of MG proceeded by cleavage of the central carbon, following with N-de-methylation process and opening of phenyl rings to form small molecular. Poulios et al. [31] proposed parallel and competing pathways between destruction of conjugated structure and N-de-methylation reactions. Although argument about proportion of different reaction routes within whole degradation is still unsolved, main degradation mechanism of MG was accomplished through decomposition of conjugated structure, accompanying with minor N-demethylation reactions and adduction reactions. Accordingly, H$_2$O$_2$-based degradation mechanism of MG under MW-enhanced condition is displayed in Scheme 1.

Decomposition of conjugated structure reaction: the oxidative degradation occurs mostly and mainly through attack on the central
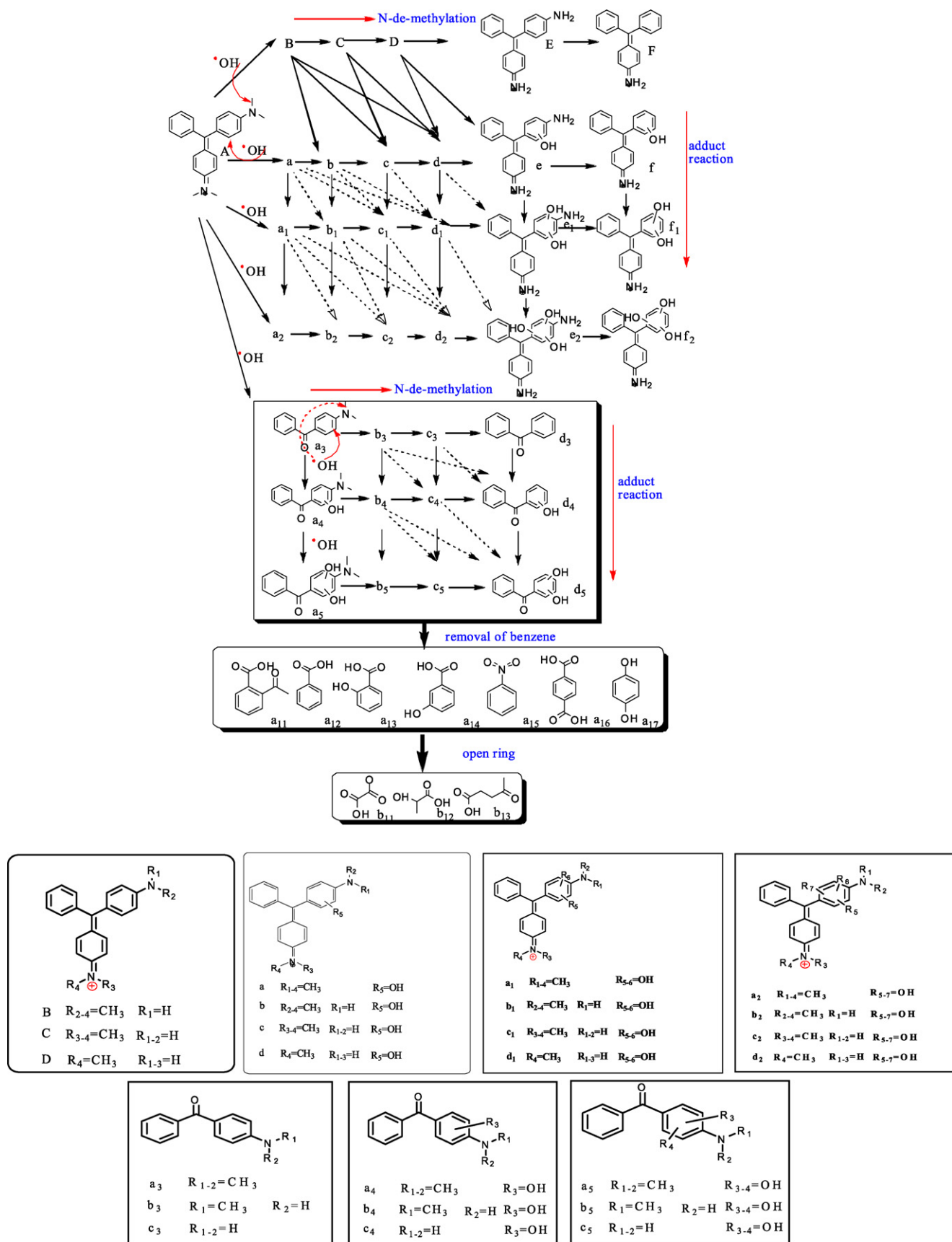
Scheme 1. Degradation mechanism of MG under MW-enhanced condition.

carbon portion of MG by •OH radicals with DLBP as main products, through which evolutions of initial dye concentration were rapidly accomplished. Furthermore, the hybrid reactions between *N*-de-methylation reactions and adduction reactions usually proceed with decomposition of central carbon of MG. Besides, under MW-enhanced condition, more radicals were available to attack all kinds of generated intermediates, which could induce adduction reactions at a ratio of *n*:1 (*n* = 1, 2, 3) between hydroxyl radicals and generated intermediates.

N-de-methylation reactions: *N*-de-methylation reactions occur mostly through nonselective attack of •OH radicals on the *N,N*-dimethyl portion of MG. Main intermediates could be observed in HPLC chromatography, detected at 618 nm. However, *N*-de-methylation reactions could not be benefit for real removal of contaminations, implying that the reaction routes were not main courses.

Adduction reactions: Under MW-enhanced condition, hydroxyl radicals could induce a series of nonselective reactions, including adduction reactions at a ratio of *n*:1 (*n* = 1, 2, 3) between hydroxyl radicals and MG. However, relative insufficient information about the structure of adduction reaction baffles further explaining the effects of adduction reactions during degradation of MG.

Removal of benzene reactions: After destruction of conjugated structure of MG, MG was further destroyed through removal of benzene reactions.

Open-ring reactions: Based on all above reactions, MG was destroyed into much small organic molecules, until eventually mineralized into CO_2 and H_2O.

5. Conclusions

The comparative results showed that MW-enhanced H_2O_2-based treatments for decomposition of conjugated structure of malachite green, was much more efficient than CH-enhanced H_2O_2-based treatment. Furthermore, according to comparative analysis about discoloration rates and intermediates, conclusion was made that microwave irradiation might be benefit for decomposition of H_2O_2 into hydroxyl radicals. Additionally, 53 kinds of intermediates were identified with LC–ESI-MS and GC–MS techniques, including 5 kinds of *N*-de-methylated intermediates, 18 kinds of intermediates formed by adduction reactions, 12 kinds of products from decomposition of conjugated structure reactions, 7 kinds of products from removal of benzene reactions, 3 kinds of inorganic acids from open-ring reactions, among which (p-dimethylaminophenyl) (p-methylaminophenyl)-phenylmethylium (DMPM), DMPPM and DLBP were identified as major intermediates. Accordingly, degradation mechanism about MG could be proposed, including: decomposition of conjugated structure reactions, *N*-de-methylation reactions, adduction reactions, removal of benzene reactions and open-ring reactions.

Acknowledgements

References

[1] M. Kaneko, I. Okura, Photocatalysis: Science and Technology, Kodansha Springer, Tokyo, Berlin, 2002.

[2] P. Pichat, Photocatalytic degradation of pollutants in water and air: basic concepts and applications, in: Chemical Degradation Methods for Wastes and Pollutants: Environmental and Industrial Applications, New York/Basel, 2003, pp. 77–119.

[3] A.G. Agrios, P. Pichat, State of the art and perspectives on materials and applications of photocatalysis over TiO_2, J. Appl. Electrochem. 35 (2005) 655–663.

[4] F.J. Beltran, Ozone-UV radiation-hydrogen peroxide oxidation technologies, in: M.A. Tarr (Ed.), Chemical Degradation Methods for Wastes and Pollutants: Environmental and Industrial Applications, Marcel Dekker Inc., New York, 2003, pp. 1–76.

[5] F.J. Benitez, F.J. Real, J.L. Acero, et al., Photochemical oxidation processes for the elimination of phenyl-urea herbicides in waters, J. Hazard. Mater. 138 (2006) 278–287.

[6] T. Yonar, K. Kestioglu, N. Azbar, Treatability studies on domestic waste-water using UV/H_2O_2 process, Appl. Catal. B-Environ. 67 (2006) 223–228.

[7] J.J. Pignatello, E. Oliveros, A. MacKay, Advanced oxidation processes for organic contaminant destruction based on the Fenton reaction and related chemistry, Crit. Rev. Environ. Sci. Technol. 36 (2006) 1–84.

[8] L.A. Pèrez-Estrada, S. Malato, W. Gernjak, et al., Photo-Fenton degradation of diclofenac: identification of main intermediates and degradation pathway, Environ. Sci. Technol. 39 (2005) 8300–8306.

[9] W. Gernjak, M. Fuerhacker, P. Fernández-Ibañez, et al., Solar photo-Fenton treatment-process parameters and process control, Appl. Catal. B-Environ. 64 (2006) 121–130.

[10] O. Legrini, E. Oliveros, A.M. Braun, Photochemical processes for water treatment, Chem. Rev. 93 (1993) 671–698.

[11] C.A.O. Nascimento, A.C.S.C. Teixeira, R. Guardani, et al., Industrial waste-water treatment by photochemical processes based on solar energy, J. Solar Energy-T ASME 129 (2007) 45–52.

[12] A.M. Braun, E. Oliveros, How to evaluate photochemical methods for water treatment, Water Sci. Technol. 35 (1997) 17–23.

[13] D. Florian, G. Knapp, High-temperature, microwave-assisted UV digestion: a promising sample preparation technique for trace element analysis, Anal. Chem. 73 (2001) 1515–1520.

[14] H. Satoshi, H. Hisao, S. Nick, Environmental remediation by an integrated microwave/UV-illumination method. II. Characteristics of a novel UV–VIS–microwave integrated irradiation device in photodegradation processes, J. Photochem. Photobiol. A: Chem. 153 (2002) 185–189.

[15] N. Ta, J. Hong, T.F. Liu, et al., Degradation of atrazine by microwave-assisted electrodeless discharge mercury lamp in aqueous solution, J. Hazard. Mater. 138 (2006) 187–194.

[16] Z.Q. Gao, S.G. Yang, N. Ta, et al., Microwave assisted rapid and complete degradation of atrazine using TiO_2 nanotube photocatalyst suspensions, J. Hazard. Mater. 145 (2007) 424–430.

[17] J. Hong, N. Ta, S.G. Yang, et al., Microwave-assisted direct photolysis of bromophenol blue using electrodeless discharge lamps, Desalination 214 (2007) 62–69.

[18] J. Hong, C. Sun, S.G. Yang, et al., Photocatalytic degradation of methylene blue in TiO_2 aqueous suspensions using microwave powered electrodeless discharge lamps, J. Hazard. Mater. 133 (2006) 162–166.

[19] Y.Z. Liu, S.G. Yang, J. Hong, et al., Low-temperature preparation and microwave photocatalytic activity study of TiO_2-mounted activated carbon, J. Hazard. Mater. 142 (2007) 208–215.

[20] S.G. Yang, H.B. Fu, C. Sun, et al., Rapid photocatalytic destruction of pentachlorophenol in F–Si-comodified TiO_2 suspensions under microwave irradiation, J. Hazard. Mater. 161 (2009) 1281–1287.

[21] Z.Q. Gao, S.G. Yang, C. Sun, et al., Microwave assisted photocatalytic degradation of pentachlorophenol in aqueous TiO_2 nanotubes suspension, Sep. Purif. Technol. 58 (2007) 24–31.

[22] Y. Sun, Y.b. Zhang, X. Quan, Treatment of Petroleum Refinery Wastewater by Microwave Assisted Catalytic Wet Air Oxidation under Low Temperature and Low Pressure, Sep. Purif. Technol. 62 (2008) 567–572.

[23] L. Lei, X. Hu, H.P. Chu, et al., Catalytic wet air oxidation of dyeing and printing wastewater, Water Sci. Technol. 35 (1997) 311–319.

[24] F.J. Zimmerann, Wet air oxidation of hazardous organic in wastewater, U.S. Patent 2, 665 (1950) 249.

[25] W.T. Wong, W.I. Chan, P.H. Liao, et al., A hydrogen peroxide/microwave advanced oxidation process for sewage sludge treatment, J. Environ. Sci. Heal. A 41 (2006) 2623–2633.

[26] G.Q. Yin, P.H. Liao, K. Victor LO, An ozone/hydrogen peroxide/microwave-enhanced advanced oxidation process for sewage sludge treatment, J. Environ. Sci. Heal A 42 (2007) 1177–1181.

[27] E. Veschetti, D. Maresca, D. Cutilli, et al., Optimization of H_2O_2 action in sewage-sludge microwave digestion using Δ pressure vs. temperature and pressure vs. time graphs, Microchem. J. 67 (2000) 171–179.

[28] P.H. Liao, K. Victorlo, W.I. Chan, et al., Sludge reduction and volatile fatty acid recovery using microwave advanced oxidation process, J. Environ. Sci. Heal A 42 (2007) 633–639.

[29] E. Cigdem, P. Audrey, M. Juan, et al., Synergetic pretreatment of sewage sludge by microwave irradiation in presence of H_2O_2 for enhanced anaerobic digestion, Water Res. 42 (2008) 4674–4682.

[30] S. Srivastava, R. Sinha, D. Roy, Toxicological effects of malachite green, Aquat. Toxicol. 66 (2004) 319–329.

[31] C. Berberidou, I. Poulios, N.P. Xekoukoulotakis, et al., Sonolytic, photo-catalytic and sonophotocatalytic degradation of malachite green in aqueous solutions, Appl. Catal. B-Environ. 74 (2007) 63–72.

[32] Y.M. Ju, S.G. Yang, Y.C. Ding, et al., Microwave assisted rapid photo-catalytic degradation of malachite green in TiO$_2$ suspensions: mechanism and pathways, J. Phys. Chem A 112 (2008) 11172–11177.

[33] B. Stoffler, G. Luft, Oxidative degradation of P-toluenesulfonic acid using hydrogen peroxide, Chemosphere 38 (1999) 1035–1047.

[34] C.S. Lu, C.C. Chen, F.D. Mai, et al., Photocatalytic degradation of Michler's ethyl ketone in titanium dioxide dispersions under UV irradiation, J. Photochem. Photobiol. A 187 (2007) 167–176.

[35] C.C. Chen, C.S. Lu, Y.C. Chung, et al., UV light induced photodegradation of malachite green on TiO$_2$ nanoparticles, J. Hazard. Mater. 141 (2007) 520–528.

[36] N. Modirshahla, M.A. Behnajady, Photooxidative degradation of malachite green (MG) by UV/H$_2$O$_2$: Influence of operational parameters and kinetic modeling, Dyes Pigments 70 (2006) 54–59.

[37] L.A. Pérez-Estrada, A. Agüera, M.D. Hernando, et al., Photodegradation of malachite green under natural sunlight irradiation: kinetic and toxicity of the transformation products, Chemosphere 70 (2008) 2068–2075.

[38] M. Cheng, W.H. Ma, J.C. Zhao, et al., Visible-light-assisted degradation of dye pollutants over Fe(III)-loaded resin in the presence of H$_2$O$_2$ at neutral pH values, Environ. Sci. Technol. 38 (2004) 1569–1575.